Solid State Ionics 383 (2022) 115978

Contents lists available at ScienceDirect

Solid State Ionics

journal homepage: www.elsevier.com/locate/ssi

Reaction kinetics in the system Y_2O_3/Al_2O_3 – Use of an external electric field to control the product phase formation in a system forming multiple product phases

Carsten Korte [a,*], Bernhard Franz [b]

[a] Institut für Energie und Klimaforschung (IEK-14: Elektrochemische Verfahrenstechnik), Forschungszentrum Jülich, 52425 Jülich, Germany
[b] Physikalisch-Chemisches Institut, Justus-Liebig Universiät Gießen, Heinrich-Buff-Ring 58, 35392 Gießen, Germany

ARTICLE INFO

Keywords:
Heterogeneous solid state reactions
Influence of an external electric field
Al_2O_3–Y_2O_3
Multiple product phases
YAG–YAP–YAM
Control of growth kinetics
Ceramic thin films

ABSTRACT

This study investigates the influence of an external electric field on the kinetics of a heterogeneous solid state reaction between Al_2O_3 and Y_2O_3. The reaction couples were prepared by means of pulsed laser deposition (PLD) by growing Y_2O_3 films on single crystalline alumina substrates with an (0001) orientation. The solid state reaction was performed at a temperature of 1400° (1673 K). Utilising attached platinum electrodes, an electric field of 350 V/mm was applied. The superposed field led to an ionic current through the reacting sample and modifies the individual growth kinetics of the three product phases/layers, $Y_3Al_5O_{12}$ (YAG), $YAlO_3$ (YAP) and $Y_4Al_2O_9$ (YAM) The cross-sections of the reacted samples were characterised by means of SEM and XRD. Depending on the direction of the ionic current, the kinetics of the YAP phase formation in particular was strongly influenced. The general kinetics of a solid state reaction forming multiple product phases was analysed using linear transport theory. The effect of an electric field for controlling the product phase formation to prefer or to kinetically suppress the formation of a distinct phase is demonstrated.

1. Introduction

Ceramic materials are utilised in many technologically-important applications such as electronics, sensor technology, energy conversion and storage, *e.g.* dielectrics, ferroelectrics, magnetic materials, insulators, solid electrolytes and mixed conductors. Solid state reactions, as degradation processes, play an important role at elevated temperatures or if an extended lifetime is required. This includes redox reactions and reactions only due to the transport of ions (or atoms), resulting in a homogeneous change in a bulk phase or the heterogeneous formation of a new product phase [1,2]. Reactive processes at internal and external interfaces in multiphase or multilayered electric or electronic devices have become a focus of research due to the ongoing drive towards miniaturisation. Solid state reactions, negligible on a macroscopic length scale, may limit the lifetime because of the short diffusion distances. Under working conditions, many devices are not only subjected to elevated temperatures but also to high electric fields due to the short distances. An electric field acts as a second driving force on mobile charge carriers and components, respectively, in addition to the chemical potential gradient.

Beyond the importance for degradation processes, the influence of an external electric field on solid state reactions has also gained more importance for the preparation of ceramic materials. In recent years, the field-assisted (flash) sintering (FAST) and spark plasma sintering (SPS) techniques were developed to a mature state and are now widely used for ceramic synthesis. An electric field is directly applied to the (green) specimen with a pair of electrodes during the sintering process, resulting in a much faster and more intense densification [3–5].

Despite the importance for thin film applications of (oxide) ceramics and bulk preparation, there have only been a limited number of basic experimental and formal studies on the influence of electric fields on the product phase formation of heterogeneous solid state reactions and their influence on the stability of microstructures [1,6–16]. In these studies, only systems were investigated forming a single product phase. This work focusses on the heterogeneous solid state reaction between alumina and yttria, simultaneously forming three product phases. The influence of an electric field on the kinetics of the product phase formation is investigated and a formal treatment is given. The electric field-assisted kinetics and product phase morphology are compared to the only thermally-driven reaction, which was investigated in detail in a

* Corresponding author.
E-mail address: c.korte@fz-juelich.de (C. Korte).

https://doi.org/10.1016/j.ssi.2022.115978
Received 25 April 2022; Received in revised form 2 June 2022; Accepted 8 June 2022
Available online 16 June 2022
0167-2738/© 2022 The Authors. Published by Elsevier B.V. This is an open access article under the CC BY license (http://creativecommons.org/licenses/by/4.0/).

previous study [17].

As has been shown in an earlier study, the superposition of an ionic flux due to an external electric field leads to a decoupling of the ionic fluxes. The growth kinetics depends now on a difference of transference numbers instead of a term with Nernst-Planck coupled conductivities as obtained for an only thermally-activated reaction [16]. In the case of a solid state reaction forming multiple product phases, this may enable (partial) control of the product phase formation. In the presence of the second driving force, the kinetically-preferred product phase may differ from that of an only thermally-activated reaction.

2. Formal considerations

2.1. Heterogeneous solid state reactions with multiple product phases

As a model for a heterogeneous solid state reaction with multiple product phases we will treat a reaction between two trivalent oxides, A_2O_3 and B_2O_3, forming a 3:5-product $A_3B_3O_{12}$, a 1:1-product ABO_3 and a 2:1-product $A_4B_2O_9$. This is a typical sequence which can be observed quite frequently for the reaction between Al_2O_3 and a rare earth sesquioxide RE_2O_3 [18–21]. The 3:5-product $A_3B_3O_{12}$ usually has a cubic garnet structure, the 1:1-product ABO_3 a (orthorhombic distorted) perovskite structure and the 2:1-product $A_4B_2O_9$ a monoclinic cuspidine structure.

For the further treatment, we denote A^{3+} and B^{3+} as general trivalent cations. For the sake of brevity, all quantities that are related to one of the product phases $A_4B_2O_9$, ABO_3 or $A_3B_5O_{12}$ will be marked with a capital letter according to their structure (M: monoclinic phase, P: perovskite and G: garnet). If all three products are formed by the starting oxides, A_2O_3 and B_2O_3, the following partial reactions will take place between the neighbouring phases in the product layer sequence, see Fig. 1a:

$$\mathrm{M}: \quad A_2O_3 + 2ABO_3 = A_4B_2O_9 \tag{1}$$

$$\mathrm{P}: \quad A_4B_2O_9 + A_3B_5O_{12} = 7ABO_3 \tag{2}$$

$$\mathrm{G}: \quad 3ABO_3 + B_2O_3 = A_3B_5O_{12} \tag{3}$$

2.2. Only thermally driven reaction

The detailed treatment of the only thermally-induced reaction using linear transport theory was presented in an earlier study [17]. It is assumed that the cations A^{2+} and B^{3+} have sufficent mobility in the product phases. The mobility of the oxide anions O^{2-}, as well as possible electronic conductivity, is neglected for the sake of simplicity, see Fig. 1a. There is no access to oxygen from the surrounding atmosphere to the phase boundaries between the starting materials and product phases and between the product phases, respectively. The treatment yields the following system of non-linear coupled ordinary differential equations (ODE) describing the simultaneous growth of the three product layers as a function of time t:

$$\frac{1}{V_m^M}\frac{d(\Delta x_M)}{dt} = \frac{k_M}{V_m^M}\frac{1}{\Delta x_M} - \frac{1}{7}\frac{k_P}{V_m^P}\frac{1}{\Delta x_P} \tag{4}$$

$$\frac{1}{V_m^P}\frac{d(\Delta x_P)}{dt} = -2\frac{k_M}{V_m^M}\frac{1}{\Delta x_M} + \frac{k_P}{V_m^P}\frac{1}{\Delta x_P} - 3\frac{k_G}{V_m^G}\frac{1}{\Delta x_G} \tag{5}$$

$$\frac{1}{V_m^G}\frac{d(\Delta x_G)}{dt} = -\frac{1}{7}\frac{k_P}{V_m^P}\frac{1}{\Delta x_P} + \frac{k_G}{V_m^G}\frac{1}{\Delta x_G} \tag{6}$$

The thickness of the product layer i is given by Δx_i and its molar volumes by V_m^i (i = M, P, G). According to Wagner and Schmalzried, k_i denotes the rate constants of the second kind, see Eq. (A.43) to (A.45) in the Appendix A [22,2,1]. The ODE system in Eq. (4) to (6) can be solved by means of simple parabolic rate laws:

$$\Delta x_M = \sqrt{2k_M'\Delta t} \tag{7}$$

$$\Delta x_P = \sqrt{2k_P'\Delta t} \tag{8}$$

$$\Delta x_G = \sqrt{2k_G'\Delta t} \tag{9}$$

This implies the introduction of rate constants of the first kind k_i'.[1] A steady-stete ratio of the product layer thicknesses Δx_M, Δx_P and Δx_G can be derived from Eq. (7) to (9) for the only thermally induced growth process:

$$\Delta x_M : \Delta x_P : \Delta x_G = \sqrt{k_M'} : \sqrt{k_P'} : \sqrt{k_G'} \tag{10}$$

2.3. Electric field assisted reaction

If an external electric field is present, acting as a second driving force on the ionic transport in the starting materials and product layers, the treatment must be modified. An ionic current is now driven through the sequence of starting materials and product layers, see Fig. 1b. Details are given in the Appendix A. The extended treatment yields a system of coupled ODEs similar to Eq. (4) to (6), but with additional terms depending on the superimposed ionic current:

$$\frac{1}{V_m^M}\frac{d(\Delta x_M)}{dt} = \frac{k_{elF}^M}{V_m^M} + \frac{k_M}{V_m^M}\frac{1}{\Delta x_M} - \frac{1}{7}\frac{k_P}{V_m^P}\frac{1}{\Delta x_P} \tag{11}$$

$$\frac{1}{V_m^P}\frac{d(\Delta x_P)}{dt} = \frac{k_{elF}^P}{V_m^P} - 2\frac{k_M}{V_m^M}\frac{1}{\Delta x_M} + \frac{k_P}{V_m^P}\frac{1}{\Delta x_P} - 3\frac{k_G}{V_m^G}\frac{1}{\Delta x_G} \tag{12}$$

$$\frac{1}{V_m^G}\frac{d(\Delta x_G)}{dt} = \frac{k_{elF}^G}{V_m^G} - \frac{1}{7}\frac{k_P}{V_m^P}\frac{1}{\Delta x_P} + \frac{k_G}{V_m^G}\frac{1}{\Delta x_G} \tag{13}$$

The newly introduced rate constants k_{elF}^i describe the influence of the additional driving force (i = M, P, G) and include the total cationic current density i_{cat} induced by the external electric field across the reacting sample:

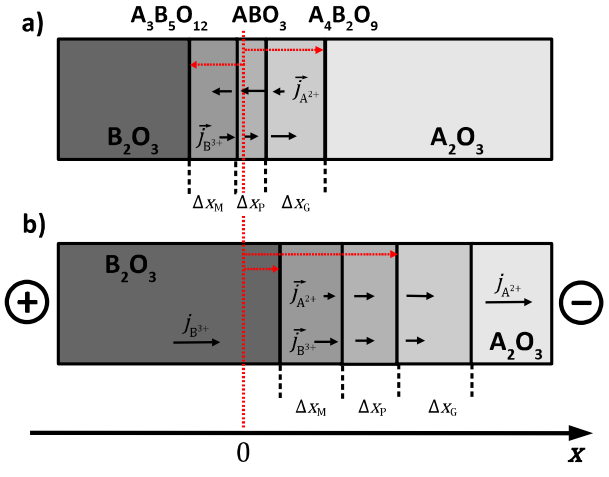

Fig. 1. Simultaneous formation of three product phases (YAM, YAP and YAG) from two starting oxides (A_2O_3 and B_2O_3) in the case of (a) an only thermally activated reaction and (b) under the influence of an external electric field. The cation fluxes $\vec{j}_{A^{3+}}$ and $\vec{j}_{B^{3+}}$ are indicated with arrows.

[1] Also called "practical" parabolic rate constants

$$k^{M}_{elF} = -\frac{i_{cat}}{3F}\left(\frac{3}{2}t^{M}_{A^{3+}} - t^{P}_{A^{3+}} - \frac{1}{2}\right)V^{M}_{m} \quad (14)$$

$$k^{P}_{elF} = \frac{i_{cat}}{3F}\left(3t^{M}_{A^{3+}} - 7t^{P}_{A^{3+}} + 4t^{G}_{A^{3+}}\right)V^{P}_{m} \quad (15)$$

$$k^{G}_{elF} = \frac{i_{cat}}{3F}\left(t^{P}_{A^{3+}} - \frac{4}{3}t^{G}_{A^{3+}}\right)V^{G}_{m} \quad (16)$$

The only thermally-induced growth is described by the rate constants k_i, as defined in Eq. (A.43) to (A.45) in the Appendix A. In contrast to the rate constants k_i, the new rate constants k^{i}_{elF} depend on the transference numbers $t^{i}_{A^{3+}}$ and $t^{i}_{B^{3+}}$ of the cations instead of the Nernst-Planck coupled partial cation conductivities.

The extended ODE system in Eq. (11) to (13) for the simultaneous growth of three product layers in the presence of an electric field cannot be solved analytically. In the case of only one product layer, an implicite analytical solution is possible using elementary functions. This is outlined for a typical spinel forming reaction in a former publication [14].

However, the following limiting cases can be distinguished for the extended ODE system in Eq. (11) to (13): *i)* Initially, if there are only very thin product layers, the additional terms depending on the external electric field can be neglected. The terms with the reciprocal layer thicknesses will dominate. Thus, the product layer growth can be approximated by parabolic rate laws as in Eq. (7) to (9), obtained for the only thermally-induced reaction:

$$\Delta x_M \approx \sqrt{2k'_M \Delta t} \quad (17)$$

$$\Delta x_P \approx \sqrt{2k'_P \Delta t} \quad (18)$$

$$\Delta x_G \approx \sqrt{2k'_G \Delta t} \quad (19)$$

ii) As the reaction proceeds, the terms with the reciprocal layer thicknesses will become ever smaller and finally the growth kinetics will only be governed by the additional terms depending on the external electric field. This yields the following linear rate laws:

$$\Delta x_M \approx k^{M}_{elF}\Delta t \quad (20)$$

$$\Delta x_P \approx k^{P}_{elF}\Delta t \quad (21)$$

$$\Delta x_G \approx k^{G}_{elF}\Delta t \quad (22)$$

This means that the growth kinetics of the product layer formation is changed by the additional electric field from parabolic rate laws to linear rate ones. The steady-state ratio of the product layer thicknesses Δx_M, Δx_P and Δx_G for the electric field driven growth process can be derived from Eq. (20) to (22):

$$\Delta x_M : \Delta x_P : \Delta x_G \approx k^{M}_{elF} : k^{P}_{elF} : k^{G}_{elF} \quad (23)$$

Thus, the electric field-assisted growth of the product layers underlies a different rate law and the steady-state ratio of the product layer thicknesses will differ compared to the only thermally-induced growth.

3. Experimental

3.1. Preparation of the thin film samples

The solid-state reaction between Al_2O_3 and Y_2O_3 was selected as a model system. A sequence of three product phases $Y_3Al_5O_{12}$ (YAG), $YAlO_3$ (YAP) and $Y_4Al_2O_9$ (YAM) is formed depending on the reaction temperature and time [23,18,19,17].

The samples were prepared using thin-film techniques. Al_2O_3 single-crystal substrates with an (0001) orientation were used (CrysTec GmbH/Berlin, 10 × 10 × 0.5 mm, epi-polished). The substrates were coated by means of pulsed laser deposition (PLD) with a Y_2O_3 film. Layers with a thickness of 6–10 μm were prepared. The substrate temperature during the deposition was adjusted to 700–900 °C. A repetition rate of 10 Hz and pulse energy of 200–250 mJ (fluence in focus 20–25 J cm^{-2}) resulted in a growth rate of 1–2 μm h^{-1}. Oxygen was used as a background gas in order to avoid non-stoichiometry in the thin film oxide (9 Pa). The Y_2O_3 targets were prepared by means of uniaxial cold pressing of Y_2O_3 powder (99.999%, Chempur/Karlsruhe) with a pressure of 60 MPa and subsequent sintering for 48 h at 1500 °C in air.

The Y_2O_3-coated Al_2O_3 substrates were post-treated in air at 800–1000 °C for 24 h in order to increase the crystallinity, see Section 3.3. The substrates were then sawn into samples of about 5 × 3 × 0.5 mm in size.

3.2. Solid state reaction

To perform the experiment with an external electric field simultaneously for both current directions, two Y_2O_3-coated Al_2O_3 substrates were attached together on the uncoated sides. Pt foils with a thickness of 0.3 mm were mechanically roughened and attached to the sides with Y_2O_3 films using platinum paste to act as electrodes. This should allow for oxygen exchange with the surrounding atmosphere (reversible electrodes). It is necessary to drive an ionic current through the sample, *e.g.* assuming predominant cation conductivity and connecting Y_2O_3 layer to the cathode side (−):

$$Al_2O_3 = 2Al^{3+} + 2/3O_2 + 6e^- \quad (24)$$

$$2Y^{3+} + 2/3O_2 + 6e^- = Y_2O_3 \quad (25)$$

The size of the electrodes (4 × 2.5 mm) was slightly smaller than the coated Al_2O_3 substrates. The two sandwiched samples were placed in a sample holder, made of Al_2O_3 oxide ceramic parts, see Fig. 2. The electric contact of the Pt electrodes was ensured with a spring loaded ceramic rod. The Pt wires were insulated using ceramic capillaries.

The same fixed temperature of 1400 °C and the same heating procedure was selected for the electric field-assisted solid state reaction as in the preceding study treating the only thermally-induced reaction

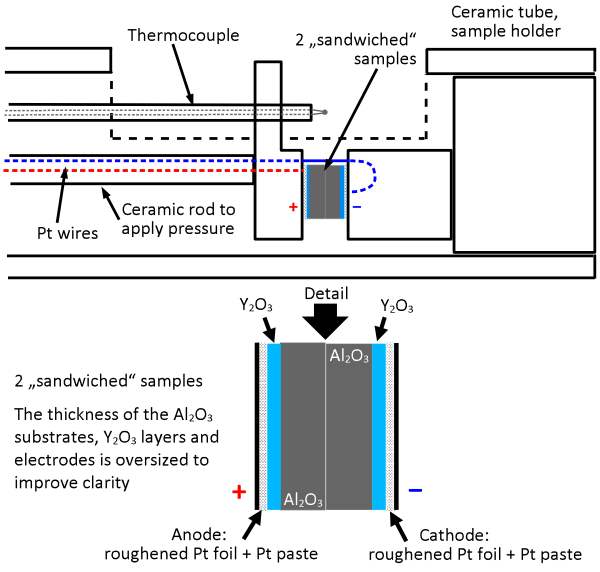

Fig. 2. Sketch of the experimental setup. The height of the Y_2O_3 thin films on the Al_2O_3/Y_2O_3 samples is oversized. Mechanical pressure to ensure the electric contact of the Pt electrodes (dotted) was applied by a spring-loaded ceramic rod. (For interpretation of the references to color in this figure legend, the reader is referred to the web version of this article.)

[17]. At this temperature, the progress of the reaction is on a timescale of hours/days and can be easily monitored by SEM, see chapter 3.3. The samples were heated up to the reaction temperature in ~60 min. by moving the sample holder into a pre-heated tubular oven and cooled down to room temperature by moving it out (20 °C /min. from room temperature to 1000 °C and 30 °C/min. from 1000 to 1400 °C). A voltage of 350 V was applied to the electrodes and the current was monitored. Reaction times between 1.5 and 72 h were chosen. The total time the samples reside in the temperature range between 1250 and 1400 °C is less than 20 min. In this temperature range, the rate constants of the thermally induced reaction will drop by two orders of magnitude according to the results by Heffelfinger et al. [24] Thus, the resulting experimental errors may be negligible.

3.3. Microstructural characterisation by XRD and SEM

The crystallinity and texture of the unreacted and reacted samples were characterised by means of X-ray diffractometry (Siemens D500, Cu-K_α, Graphite diffracted beam monochromator, Bragg-Brentano geometry). The morphological development of the product layer were characterised by using scanning electron microscopy (SEM, LEO Gemini 982). The cross-sections of the reacted samples were prepared by means of mechanical polishing. The final polishing step was carried out using colloidal silicon oxide (0.01 μm). The SEM images were taken in back-scattered electron mode (BSE) at 10 kV acceleration voltage in order to achieve an optimal contrast between the individual phases Al_2O_3, YAG, YAP, YAM and Y_2O_3.

4. Results

4.1. Structural characterisation of the Y_2O_3 thin film

Dense and continuous Y_2O_3 films with a thickness of up to 10 μm can be grown by PLD on Al_2O_3 substrates. No voids can be detected by SEM in the unreacted Y_2O_3 phase. The details regarding the texture and crystallinity of the unreacted samples can be found in the preceding study on the only thermally initiated reaction [17].

According to the results of the XRD characterisation, the as-deposited films have poor crystallinity. Thus, a thermal treatment at 800–1000 °C was performed (FMWH of ~0.8 ° before and ~0.5 ° after, no detectable formation of product phases). When investigating samples with different film thicknesses, it became apparent that the crystallites in a Y_2O_3 thin film are initially grown in a (111) orientation on a (0001) Al_2O_3 substrate. With increasing film thickness, the subsequently formed crystallites prefer the (110) orientation.

4.2. Morphology of the product layers

In order to analyse the moving phase boundaries, the cross-sections of the samples reacted under the influence of an electric field were characterised by SEM. The results were compared to those of the preceding study, treating the only thermally induced reaction [17].

The grain boundary structure is only partially visible using the BSE imaging mode. Due to the differing hardness of the ceramic substrate, layers and electrodes, significant scratches on the surface resulting from the sample preparation affect the SEM analysis when considering the channeling contrast. It can be discerned in Fig. 3 that the grain boundaries, respectively the individual grains in the YAG and YAP product phase are connected across the phase boundary. In the case of the YAP phase, a uniform layer thickness was only present at very short reaction times. When the reaction proceeds, significant thickness variations appear for the reference, as well as when applying an (external) electric field.

If the Y_2O_3 layer is aligned to the anode (+) side, the morphology of the product phases and their interfaces is comparable to the results found for the reference without a field, see Fig. 4a and b. However, there is a significantly increased wavyness of the Al_2O_3/YAP interface. A

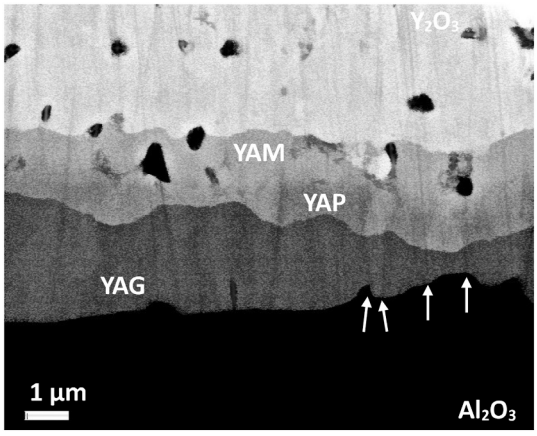

Fig. 3. Contrast enhanced and de-noised SEM microslide (cross section, 10 kV acceleration voltage, BSE mode) of of a sample after a reaction time of 16 h (T = 1400 °C). The Y_2O_3 layer is connected to the anode side (+), applying a potential difference of 350 V. The grain boundaries ('arrows') are partially visible due to channeling contrast.

formation of pores could be observed in the Y_2O_3/YAM interface. To a smaller extent, this is also noticeable in the YAM/YAP interface.

If the Y_2O_3 layer is on the cathode (−) side, the morphology of the product phases and their interfaces differs significantly when compared to the reference without field and to anodic polarisation, see Fig. 4a and c. The observed pore formation is even stronger compared to the anodic polarisation. Pores are not only in the Y_2O_3/YAM, but also in the Al_2O_3/YAP interface. Generally, the pore formation hampers the determination of the product layer thicknesses, resulting in increased experimental errors. The strong pore formation in the case of cathodic polarisation partially results in heavily damaged cross sections, due the mechanical stress during the polishing process, see Fig. 4c at 7 h, 46 h and 72 h.

4.3. Growth kinetics

A current of about 3 mA can be measured nearly during the whole experimental time, when applying a voltage of 350 V to the sandwiched samples. Considering the area of the electrodes of $1.0 \cdot 10^{-1}$ cm^2 and the distance of 1 mm, this corresponds to a current density of 30 mA cm^{-2} and an average electric field of 3.5 kV cm^{-1}. According to the literature, the (total) conductivity of Al_2O_3 at 1400 °C is in the order of 10^{-6} to 10^{-7} S cm^{-1}. Values of about 10^{-4} S cm^{-1} can be found for Y_2O_3 [25–32]. This indicates that the electric field in the Y_2O_3 thin film is probably about 3 orders of magnitude smaller than the estimated average. However, the (total) conductivities of the product phases are much closer to the value found for Al_2O_3 and thus also the magnitude of the electric field [17,33]. A value of $6.3 \cdot 10^{-7}$ S cm^{-1} can be found for YAG.

The average product layer thicknesses Δx_i (i = M, P and G) were evaluated from the SEM microslides using the software ImageJ [34]. The errors were estimated according to the observed variations when performing the image analysis at different locations, *i.e.* according to the observed thickness variations. The results for the samples, reacted by applying an electric potential difference of 350 V and connecting the Y_2O_3 layer to the anode (+) or cathode (−), are depicted in Fig. 5. A double logarithmic scaling was used to plot the relation between the thickness Δx_i of the product layer i and reaction time Δt. For comparison, the results of the reference sample reacted without an applied voltage are also provided [17]. The data is fitted by using a general power function $\Delta x_i = a\,(\Delta t)^b$. The results for the fit parameters are listed in Table 1.

In general, the growth rates of the product phases are increasing in the order YAP ≪ YAM < YAG. This is the case with and without applying an electric potential difference. The growth rate of the YAP phase is nearly one order of magnitude lower compared to the YAG phase.

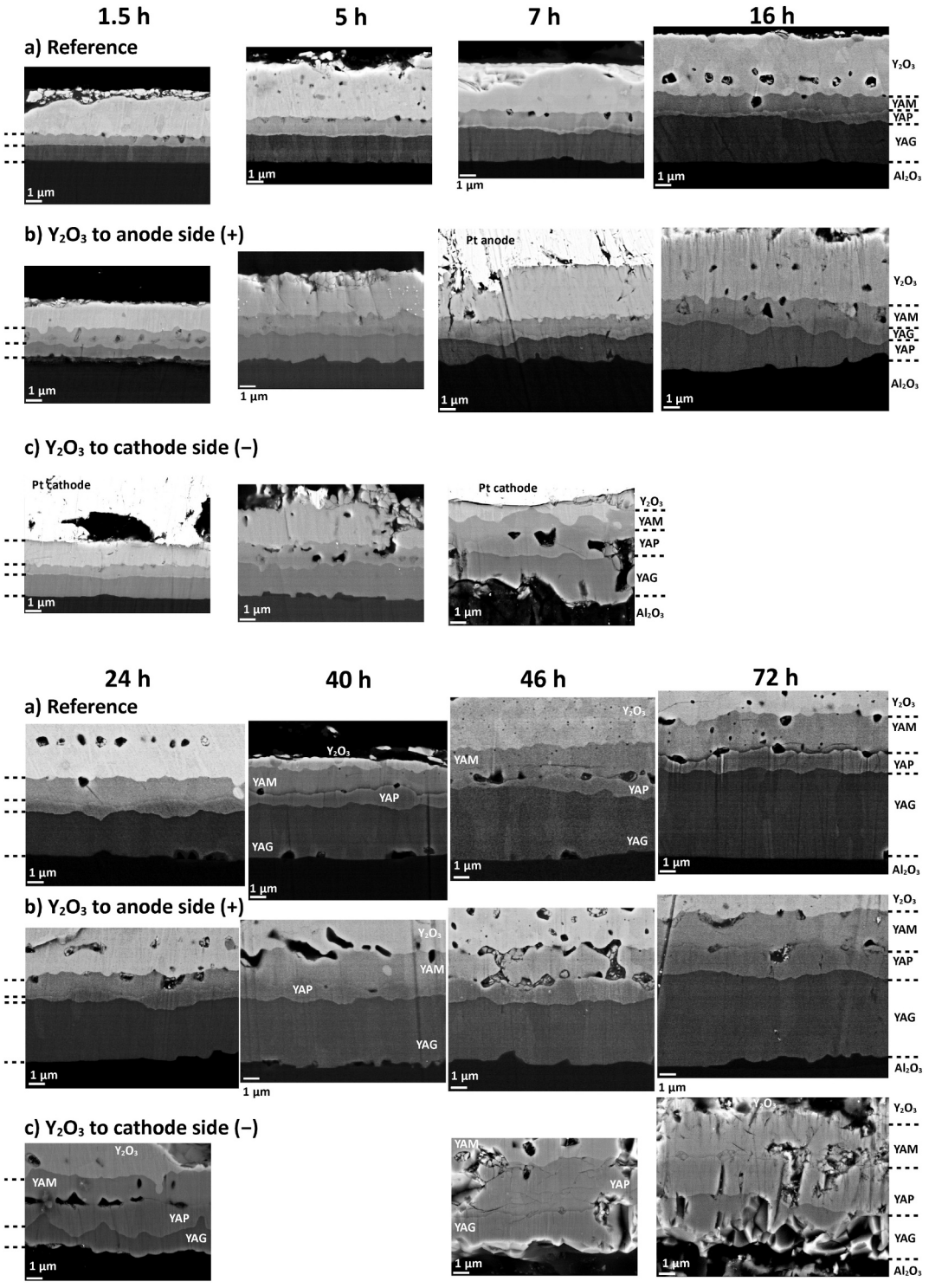

Fig. 4. SEM microslides (cross sections, 10 kV acceleration voltage, BSE mode) of different samples after a reaction time of 1.5 h, 5 h, 7 h, 16 h, 24 h, 40 h 46 h and 72 h ($T = 1400$ °C). The microslides of the reference samples (a) without electric field are taken from the preceding study [17]. An electic potential difference of 350 V is applied to the samples denoted with (b) and (c), whereas in the first case the Y_2O_3 layer is connected to the anode side (+) and in the latter case to the cathode side (−).

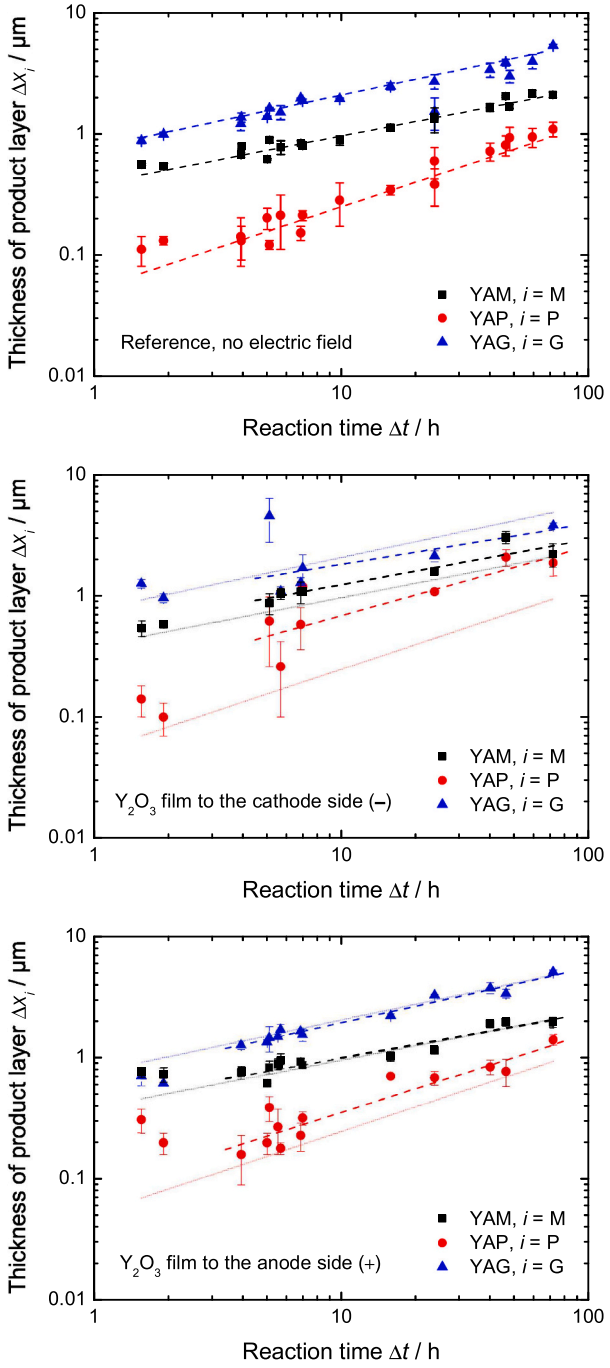

Fig. 5. Double logarithmic plots of the product layer thickness Δx_i *vs.* reaction time Δt. From top to bottom: reference without electric field, Y_2O_3 film to the cathode side (−)and Y_2O_3 film to the anode side (+). The dashed lines were obtained by fitting a general power function $\Delta x_i = a\ (\Delta t)^b$. The obtained fit parameters are listed in Table 1. The light solid lines in the middle and bottom plots are the fit curves obtained for the reference (top plot).

5. Discussion

5.1. Orientation of the deposited Y_2O_3 layers

Y_2O_3 has a cubic bixbyite structure ($Ia\bar{3}$) and the Al_2O_3 substrate a trigonal corundum structure ($R\bar{3}c$). There is a preference for the nucleation and growth of the Y_2O_3 crystallites in a (111) orientation on a (0001) Al_2O_3 substrate according to the trifold symmetry axis perpendicular to the substrate plane/growth direction. With increasing film thickness, crystallites with other orientations will also nucleate. This was discussed in more detail in the preceding study about the only thermally-initiated reaction [17].

Table 1
Result from fiting the experimental data with a general power function $\Delta x_i = a\ (\Delta t)^b$. If $b = 1/2$, the prefactor a is equal to $\sqrt{2k_i}$, if $b = 1$ the prefactor a is equal to k^i_{elF}

Polarity	Prefactor a / $(10^{-2} \cdot \mu m\ h^{-b})$			Exponent b / 1		
	YAM	YAP	YAG	YAM	YAP	YAG
Reference, no electric field	39.6 ± 2.3	5.23 ± 0.63	73.5 ± 9.5	0.40 ± 0.02	0.71 ± 0.04	0.40 ± 0.04
(−), Y_2O_3 film to cathode side	52.1 ± 12.4	18.4 ± 8.7	84.3 ± 54.2	0.38 ± 0.07	0.57 ± 0.14	0.33 ± 0.22
(+), Y_2O_3 film to anode side	43.1 ± 4.9	7.91 ± 1.71	69.4 ± 5.5	0.37 ± 0.04	0.65 ± 0.07	0.45 ± 0.03

5.2. Morphology of the product layers

As the observed wavyness of the Y_2O_3/YAM and Al_2O_3/YAG interface, *i.e.* the triangular-like features are usually accompanied to grain boundaries in the adjacent phases, they might be caused by enhanced mass transport along these boundaries and by a preferential nucleation of the product phases at the end of the grain boundaries in the initial Y_2O_3 layer. Unfortunately, the grain boundary structure in the YAG, YAP, YAM and Y_2O_3 phases is difficult to discern in the SEM/BSE microslides, see Fig. 3, 'arrows'. However, a match with the triangular-like features in the interface is partially possible.

These phenomena are frequently present in thermally-initiated heterogeneous solid state reactions. It was discussed in more details in the preceding study on the reaction of Y_2O_3 and Al_2O_3 [17,24]. The increased wavyness of the Al_2O_3/YAG interface, observed for the samples reacted under the influence of an electrical potential difference, may be caused by the superposed ionic current and an increasing influence of grain boundary transport. This was also observed for the electric field enhanced reaction of In_2O_3 and MgO [11,16].

The observed pore formation in the interface between the Y_2O_3 and YAM phase, respectively in the bulk of the Y_2O_3 phase, is most likely due to the presence of electronic conductivity at the high reaction temperature. As reported by Schmalzried and Pfeiffer, a running solid state reaction will cause the build-up of an oxygen partial pressure gradient in the presence of electronic conductivity, resulting in the formation of voids at grain and phase boundaries [35].

5.3. Growth kinetics

The voltage applied to the sandwiched samples results in an electric field of 3.5 kV cm^{-1}. Using this value and the measured current density of 30 mA cm^{-1}, a conductivity of about $8.6 \cdot 10^{-7}$ S cm^{-1} can be estimated. Due to the thickness ratio between both thin films and both Al_2O_3 substrates in the sandwiched samples (~10 µm: 1 mm), the charge transport is primarily governed by the properties of single crystalline Al_2O_3. In the literature, the values found for the total conductivity of Al_2O_3 were spread between 10^{-7}–10^{-6} S cm^{-1} [27–32]. If grain boundaries are present (polycrystalline samples), the given upper limit will be reached. Taking into account the fact that no guard electrodes are used to prevent surface conduction, this indicates for a single-crystal substrates that the true total current density may be one order of magnitude lower, *i.e.* i_{tot}~10^{-3} A cm^{-1}.

The values of the transference numbers in Al_2O_3 are not fully clear. According to Brook et al. and Yee et al., the electronic transference number t_{el} decreases with temperature, estimating a $t_{ion} = 1 - t_{el}$ of about 1 below 1400 °C [28,29]. The opposite was reported by Will et al. [30]. Only a value of 0.02 to 0.04 is reported for t_{ion} at a temperature of 1300 °C. The dominating charge carrier, responsible for the ionic

transport $t_{ion} = t_{Al^{3+}} + t_{O^{2-}}$, was also controversially discussed. The ratio of $t_{Al^{3+}}$ and $t_{O^{2-}}$ may also depend on the oxygen partial pressure p_{O_2} and the presence of grain boundaries (polycrystalline samples) [32]. Considering the results on the transference numbers from the literature and the very likely presence of surface conduction, the cationic current density $i_{cat} < i_{ion} = i_{tot} - i_{el}$ is presumabely in the order of 10^{-5} A cm^{-1}.

The reaction system Y_2O_3/Al_2O_3, forming three product phases, can be described by a system of three ODEs, see Eq. (4) to (6) (only thermally initated reaction) and Eq. (11) to (13) (with a superimposed ionic current/external electric field). According to the limiting cases discussed in the formal considerations, a change from a parabolic growth law to a linear one should appear if an external electric field is present, see Eq. (17) and (22). Using a double-logarithmic plot for the data, *i.e.* Δx_i *vs.* Δt, the change in the rate law can be proven by a change in the slope from 1/2 in the case of the only thermally-initiated reaction to 1 in the presence of an electric field.

In Fig. 5 the thickness changes Δx_i of the products layers in the reaction system Al_2O_3/Y_2O_3 are depicted for different field (current) directions and for the only thermally-initiated reference (double-logarithmic plot). The growth rates can be analysed by fitting general power functions $\Delta x_i = a\,(\Delta t)^b$, see Table 1. It becomes apparent that the effect of the applied electric field is less pronounced compared to preceding studies on the reaction system In_2O_3/MgO that forms only a single product layer of $MgIn_2O_4$ [11,16].

Using linear transport theory, the growth of a single product layer can be described by a single ODE. As well, a change from a parabolic growth law to a linear one should appear if an external electric field is present. An increased growth of the product phase can be expected if the trivalent oxide is connected to the cathode (−) side and the transference number of the divalent cation is higher compared to the trivalent cation [16]. Both can be confirmed for the In_2O_3/MgO system, see the (double-logarithmic) plot in the supplemental material of the product phase thickness $\Delta x_{MgIn_2O_4}$ *vs.* reaction time Δt. By fitting a general power function $\Delta x_{MgIn_2O_4} = a\,(\Delta t)^b$, a slope of 0.50±0.06 can be found for the only thermally-initiated reaction and of 1.10±0.11 for the electric field driven reaction. In the presence of an electric field, there is no detectable change in the slope with the reaction time or in the product layer thickness, respectively. Presumably, the change from diffusion to electric field control will appear in the very beginning of the reaction, which is difficult to access by fast quenching and *ex-situ* analysis of the samples.

In the case of the reaction system Y_2O_3/Al_2O_3 it was not possible to detect a systematic change in the slope when comparing the only thermally-reacted reference to the samples reacted under the influence of an (external) electric field or a change of the growth kinetic with time under the influence of an elecric field. A value always in the order of 0.4 can be found in the YAM and YAG phase and a value always in the order of 0.6 to 0.7 in the YAP phase, see Table 1.

There is no clear effect of the (external) electric field on the growth rate of the YAG phase. The growth rate when connecting the Y_2O_3 layer to the cathode side (−) or when connecting it to the anode side (+) does not significantly differ from the reference without external field (ratio of prefactors: $a(-)/a(\text{Ref}) \approx 1.15$, $a(+)/a(\text{Ref}) \approx 0.94$), see Fig. 5 and Table 1. A very slight increase of the growth rate is present for the YAM phase (ratio of prefactors: $a(-)/a(\text{Ref}) \approx 1.32$, $a(+)/a(\text{Ref}) \approx 1.09$) and a significant effect can be observed for the YAP phase (ratio of prefactors: $a(-)/a(\text{Ref}) \approx 3.52$, $a(+)/a(\text{Ref}) \approx 1.51$), when connecting the Y_2O_3 layer to the cathode side (−). However, there are significant experimental errors in the thickness measurements when applying an electric field due to pore formation and irregular wavy reaction fronts, especially for this polarity.

Considering the above observations that the effect of the (external) electric field is negligable for the YAG and YAM phases, it is possible to estimate the ionic transference numbers $t^i_{Y^{3+}}$ and $t^i_{Al^{3+}}$ in the product phases (i = M, P and G) at the experimental temperature of 1400 °C to be consistent with this. The transference numbers in the YAG phase can be obtained from the measured value of the Nernst-Planck coupled conductivity $\sigma^G_{Y^{3+}}\sigma^G_{Al^{3+}}/(\sigma^G_{Y^{3+}} + \sigma^G_{Al^{3+}})$ from the preceding study ($3.55 \cdot 10^{-8}$ S cm^{-1}) and the total cationic conductivity $\sigma^G_{Y^{3+}} + \sigma^G_{Al^{3+}}$ at 1400 ° from Bates and Garnier ($6.3 \cdot 10^{-7}$ S cm^{-1}) [33,17]. This yields a value of about 0.06 for $t^G_{Y^{3+}}$. Using Eq. (14) to (16) (A = Y, B = Al) and assuming that k^M_{elF} and k^G_{elF} are at least ten times smaller than k^P_{elF} results in a system of inequations and yields that $t^P_{Y^{3+}}$ should be in the order of 0.08–0.1 and $t^M_{Y^{3+}}$ in the order of 0.39 (see supplemental material). This corresponds to cation conductivities in the order of 10^{-8} S cm^{-1} for the YAM phase and of 10^{-9}–10^{-8} S cm^{-1} for the YAP phase.

Taking a total cationic current density *icat* in the order of 10^{-5} A cm^2 into account, this would result in values for k^G_{elF} and k^M_{elF} for the YAG and YAM phases much too low to influence the only thermally driven growth rates. It does not explain the missing change of the kinetics (exponent) for the growth of the YAP phase. However, these are only very rough estimations, as a possible O^{2-} conduction is neglected in the model (see Appendix A) and the possible built-up of an oxygen partial pressure gradient (see pore formation) is not taken into account. The latter might also have an influence on the cationic transport processes.

6. Summary

As an extension of the preceding study on the only thermally-driven solid state reaction between two sequioxides A_2O_3–B_2O_3, the formalisms of Wagner and Schmalzried can also be applied to the general treatment in the case of the additional influence of an external electric field. Likewise, it is assumed that the heterogeneous reaction forms three product phases, namely a garnet phase ($A_5B_3O_{12}$), a perovskite phase (ABO_3) and a cuspidin phase ($A_4B_2O_9$). The treatment using linear transport theory yields a transition between a diffusion-limited parabolic growth law to a electric field driven linear growth law for the coupled formation of the product phases. The growth rates of the products phase will depend on the differences in the cationic transference numbers instead of the Nernst-Planck-coupled conductivities. This is comparable to the results from a former study on the spinel forming reaction system AO–B_2O_3.

When comparing the reaction of the sequioxide system Al_2O_3–Y_2O_3 at 1400 °C under the influence of an electric field to the reference reaction without a field, an enhanced formation of the perovskite (YAP) phase can be observed if the Y_2O_3 phase is connected to the cathode (−) side. In the case of the opposite polarity of the electric field and regarding the other product phases, YAG and YAM, the effect is negligible. This demonstrates that the product phase preferentially formed by a solid state reaction can be kinetically influenced by applying an electric field.

Surprisingly, there is no significant change in the growth kinetics, *i.e.* the exponents observed for the rate laws do not change significantly when applying an electric field. In the case of the YAG and YAM product phases the value is in the order of a diffusion-limited parabolic growth law (~0.4). In the case of the YAP phase, the value is distinctly higher than 1/2, but is also independent of the presence of an electric field. In the case of the YAM and YAG phases, this might be explained by a ratio of the cationic transference numbers leading to an negligible influence of the electric field-induced ionic transport on the total growth rate. However, this does not hold in the case of the YAP phase as enhanced growth can be observed.

For the sake of simplicity, the suggested model does not include a possible O^{2-} conduction, which may change the relevant interface reactions and does not take the possible build-up of an oxygen partial pressure gradient into account. Both may also modify the kinetics. A more suitable model system to investigate these phenomena should react at significantly lower temperatures in order to avoid experimental complications like surface and electronic conduction.

Declaration of Competing Interest

Carsten Korte reports that financial support was provided by the German Research Foundation.

Acknowledgment

We are grateful to the German Science Foundation (DFG, Ko1859/2-1) and the State of Hessen for financial support (BF and CK).

Appendix A. The reaction system A_2O_3–B_2O_3 in the presence of an external electric field

A.1. Linear transport theory

The following treatment is restricted to an one-dimensional system, see Fig. 1b. All vector quantities such as the ionic fluxes and electrochemical potential gradients are treated as scalars. A positive sign corresponds to a vector in the direction of the $+x$-axis and a negative to a vector in the opposite direction. There will always be a linear dependence between the driving forces and the induced fluxes. The transport coefficients are assumed to be concentration independent.

A.2. Condition of electroneutrality

The cation fluxes $j^i_{A^{3+}}$ and $j^i_{B^{3+}}$ in the three product phases (i = M, P or G) and the starting material ($i = A_2O_3$, B_2O_3) are driven by the external electric field. The simultaneous fluxes of the A^{3+} and B^{3+} cations in the product phases are coupled by the condition of charge conservation and the sum of the flown charge is equal to the total cationic current density i_{cat} through the reacting system, see Fig. 1b:

$$A_2O_3: \quad 3Fj^{A_2O_3}_{A^{3+}} = i_{cat} \tag{A.1}$$

$$M: \quad 3Fj^{M}_{A^{3+}} + 3Fj^{M}_{B^{3+}} = i_{cat} \tag{A.2}$$

$$P: \quad 3Fj^{P}_{A^{3+}} + 3Fj^{P}_{B^{3+}} = i_{cat} \tag{A.3}$$

$$G: \quad 3Fj^{G}_{A^{3+}} + 3Fj^{G}_{B^{3+}} = i_{cat} \tag{A.4}$$

$$B_2O_3: \quad 3Fj^{B_2O_3}_{A^{3+}} = i_{cat} \tag{A.5}$$

There is only a flux of A^{3+} cations in the starting material A_2O_3 and of B^{3+} cations in B_2O_3. There are no O^{2-} and electronic fluxes. If present, these would lead to additional terms in Eq. (A.1) to (A.5) and also to modified partial reactions at the interfaces in Eq. (A.6) to (A.9), now including O^{2-} ions as reaction partners.

A.3. Growth rate of the product phases

According to the partial reactions in Eq. (1) to (3) and the cation fluxes in the product layers driving the mass transport, the following reactions will drive the motion of the phase boundaries:

$$M/A_2O_3: \quad A_4B_2O_9 + 2A^{3+} = 3A_2O_3 + 2B^{3+} \tag{A.6}$$

$$P/M: \quad 3ABO_3 + A^{3+} = A_4B_2O_9 + B^{3+} \tag{A.7}$$

$$G/P: \quad A_3B_5O_{12} + A^{3+} = 4ABO_3 + B^{3+} \tag{A.8}$$

$$B_2O_3/G: \quad 4B_2O_3 + 3A^{3+} = A_3B_5O_{12} + 3B^{3+} \tag{A.9}$$

Considering the coupling of the cation fluxes to the total ionic current density in Eq. (A.1) to (A.5) and the stoichiometries in Eq. (A.6) to (A.9), the relative velocities of the phase boundaries of the product layers can be derived. This yields for the monoclinic phase (M):

$$v^{M}_{P/M} = V^{M}_{m}\left(j^{M}_{A^{3+}} - j^{P}_{A^{3+}}\right) = -V^{M}_{m}\left(j^{M}_{B^{3+}} - j^{P}_{B^{3+}}\right) \tag{A.10}$$

$$v^{M}_{M/A_2O_3} = -\frac{1}{2}V^{M}_{m}\left(j^{M}_{A^{3+}} - j^{A_2O_3}_{A^{3+}}\right) = \frac{1}{2}V^{M}_{m}j^{M}_{B^{3+}} \tag{A.11}$$

and for the perovskite phase (P):

$$v^{\mathrm{P}}_{\mathrm{G/P}} = 4V^{\mathrm{P}}_{\mathrm{m}}\left(j^{\mathrm{P}}_{\mathrm{A}^{3+}} - j^{\mathrm{G}}_{\mathrm{A}^{3+}}\right) = -4V^{\mathrm{P}}_{\mathrm{m}}\left(j^{\mathrm{P}}_{\mathrm{B}^{3+}} - j^{\mathrm{G}}_{\mathrm{B}^{3+}}\right) \tag{A.12}$$

$$v^{\mathrm{P}}_{\mathrm{P/M}} = 3V^{\mathrm{P}}_{\mathrm{m}}\left(j^{\mathrm{M}}_{\mathrm{A}^{3+}} - j^{\mathrm{P}}_{\mathrm{A}^{3+}}\right) = -3V^{\mathrm{P}}_{\mathrm{m}}\left(j^{\mathrm{M}}_{\mathrm{B}^{3+}} - j^{\mathrm{P}}_{\mathrm{B}^{3+}}\right) \tag{A.13}$$

and for the garnet phase (G):

$$v^{\mathrm{G}}_{\mathrm{B_2O_3/G}} = \frac{1}{3}V^{\mathrm{G}}_{\mathrm{m}} j^{\mathrm{G}}_{\mathrm{A}^{3+}} = -\frac{1}{3}V^{\mathrm{G}}_{\mathrm{m}}\left(j^{\mathrm{G}}_{\mathrm{B}^{3+}} - j^{\mathrm{B_2O_3}}_{\mathrm{B}^{3+}}\right) \tag{A.14}$$

$$v^{\mathrm{G}}_{\mathrm{G/P}} = V^{\mathrm{G}}_{\mathrm{m}}\left(j^{\mathrm{P}}_{\mathrm{A}^{3+}} - j^{\mathrm{G}}_{\mathrm{A}^{3+}}\right) = -V^{\mathrm{G}}_{\mathrm{m}}\left(j^{\mathrm{P}}_{\mathrm{B}^{3+}} - j^{\mathrm{G}}_{\mathrm{B}^{3+}}\right) \tag{A.15}$$

The O^{2-} sublattices of the product phases are assumed to be a rigid reference frames. The growth rate of a certain product phase is calculated from the difference in the phase boundary velocities. This yields for the monoclinic phase (M):

$$\frac{1}{V^{\mathrm{M}}_{\mathrm{m}}}\frac{\mathrm{d}(\Delta x_{\mathrm{M}})}{\mathrm{d}t} = -\left(\frac{3}{2}j^{\mathrm{M}}_{\mathrm{A}^{3+}} - j^{\mathrm{P}}_{\mathrm{A}^{3+}} - \frac{1}{2}j^{\mathrm{A_2O_3}}_{\mathrm{A}^{3+}}\right) = \frac{3}{2}j^{\mathrm{M}}_{\mathrm{B}^{3+}} - j^{\mathrm{P}}_{\mathrm{B}^{3+}} \tag{A.16}$$

and for the perovskite phase (P):

$$\frac{1}{V^{\mathrm{P}}_{\mathrm{m}}}\frac{\mathrm{d}(\Delta x_{\mathrm{P}})}{\mathrm{d}t} = 3j^{\mathrm{M}}_{\mathrm{A}^{3+}} - 7j^{\mathrm{P}}_{\mathrm{A}^{3+}} + 4\overrightarrow{j}^{\mathrm{G}}_{\mathrm{A}^{3+}} = -\left(3j^{\mathrm{M}}_{\mathrm{B}^{3+}} - 7j^{\mathrm{P}}_{\mathrm{B}^{3+}} + 4j^{\mathrm{G}}_{\mathrm{B}^{3+}}\right) \tag{A.17}$$

and for the garnet phase (G):

$$\frac{1}{V^{\mathrm{G}}_{\mathrm{m}}}\frac{\mathrm{d}(\Delta x_{\mathrm{G}})}{\mathrm{d}t} = j^{\mathrm{P}}_{\mathrm{A}^{3+}} - \frac{4}{3}j^{\mathrm{G}}_{\mathrm{A}^{3+}} = -\left(j^{\mathrm{P}}_{\mathrm{B}^{3+}} - \frac{4}{3}j^{\mathrm{G}}_{\mathrm{B}^{3+}} + \frac{1}{3}j^{\mathrm{B_2O_3}}_{\mathrm{B}^{3+}}\right) \tag{A.18}$$

The formal treatment to obtain Eq. (A.16) to (A.18) is the same as for the only thermally-driven reaction [17].

A.4. Diffusive charge transport

The ionic transport is driven by electrochemical potential gradients in the product phases and can be described by linear transport equations (i = M, P, G):

$$j^{i}_{\mathrm{A}^{3+}} = -\frac{\sigma^{i}_{\mathrm{A}^{3+}}}{(3F)^2}\frac{\mathrm{d}\tilde{\mu}^{i}_{\mathrm{A}^{3+}}}{\mathrm{d}x} \tag{A.19}$$

$$j^{i}_{\mathrm{B}^{3+}} = -\frac{\sigma^{i}_{\mathrm{B}^{3+}}}{(3F)^2}\frac{\mathrm{d}\tilde{\mu}^{i}_{\mathrm{B}^{3+}}}{\mathrm{d}x} \tag{A.20}$$

The partial cation conductivities in the product phase i are denoted with $\sigma^{i}_{\mathrm{A}^{3+}}$ and $\sigma^{i}_{\mathrm{B}^{3+}}$. For the further treatment, the electrochemical potential gradients $\mathrm{d}\tilde{\mu}^{i}_{\mathrm{A}^{3+}}/\mathrm{d}x$ and $\mathrm{d}\tilde{\mu}^{i}_{\mathrm{B}^{3+}}/\mathrm{d}x$ of the cations must be expressed by directly measurable values, *i.e.* the chemical potential gradients of components A_2O_3 and B_2O_3:

$$\mathrm{M}: \quad \frac{\mathrm{d}\tilde{\mu}^{\mathrm{M}}_{\mathrm{A}^{3+}}}{\mathrm{d}x} - \frac{\mathrm{d}\tilde{\mu}^{\mathrm{M}}_{\mathrm{B}^{3+}}}{\mathrm{d}x} = \frac{3}{2}\frac{\mathrm{d}\mu^{\mathrm{M}}_{\mathrm{A_2O_3}}}{\mathrm{d}x} = -\frac{3}{4}\frac{\mathrm{d}\mu^{\mathrm{M}}_{\mathrm{B_2O_3}}}{\mathrm{d}x} \tag{A.21}$$

$$\mathrm{P}: \quad \frac{\mathrm{d}\tilde{\mu}^{\mathrm{P}}_{\mathrm{A}^{3+}}}{\mathrm{d}x} - \frac{\mathrm{d}\tilde{\mu}^{\mathrm{P}}_{\mathrm{B}^{3+}}}{\mathrm{d}x} = \frac{\mathrm{d}\mu^{\mathrm{P}}_{\mathrm{A_2O_3}}}{\mathrm{d}x} = -\frac{\mathrm{d}\mu^{\mathrm{P}}_{\mathrm{B_2O_3}}}{\mathrm{d}x} \tag{A.22}$$

$$\mathrm{G}: \quad \frac{\mathrm{d}\tilde{\mu}^{\mathrm{G}}_{\mathrm{A}^{3+}}}{\mathrm{d}x} - \frac{\mathrm{d}\tilde{\mu}^{\mathrm{G}}_{\mathrm{B}^{3+}}}{\mathrm{d}x} = \frac{4}{5}\frac{\mathrm{d}\mu^{\mathrm{G}}_{\mathrm{A_2O_3}}}{\mathrm{d}x} = -\frac{4}{3}\frac{\mathrm{d}\mu^{\mathrm{G}}_{\mathrm{B_2O_3}}}{\mathrm{d}x} \tag{A.23}$$

For details, see the preceding publication [17]. Using Eq. (A.21) to (A.23) and the coupling of the cation fluxes to the total ionic current density in Eq. (A.2) to (A.4), the cation fluxes in Eq. (A.19) and (A.20) can be rewritten in a way that the chemical potential gradients of components A_2O_3 and B_2O_3 appear as driving forces. This yields for the monoclinic phase (M)[2]:

[2] For the sake of brevity the (cationic) transference numbers are introduced as (i = M, P or G):

$$t^{i}_{\mathrm{A}^{3+}} = \frac{\sigma^{i}_{\mathrm{A}^{3+}}}{\sigma^{i}_{\mathrm{A}^{3+}} + \sigma^{i}_{\mathrm{B}^{3+}}} \quad \text{and} \quad t^{i}_{\mathrm{B}^{3+}} = \frac{\sigma^{i}_{\mathrm{B}^{3+}}}{\sigma^{i}_{\mathrm{A}^{3+}} + \sigma^{i}_{\mathrm{B}^{3+}}} \tag{A.24}$$

$$j^{M}_{A^{3+}} = t^{M}_{A^{3+}}\frac{i_{cat}}{3F} - \frac{3}{2}\frac{1}{(3F)^2}t^{M}_{A^{3+}}\sigma^{M}_{B^{3+}}\frac{d\mu^{M}_{A_2O_3}}{dx} \tag{A.25}$$

$$j^{M}_{B^{3+}} = t^{M}_{B^{3+}}\frac{i_{cat}}{3F} - \frac{3}{4}\frac{1}{(3F)^2}t^{M}_{A^{3+}}\sigma^{M}_{B^{3+}}\frac{d\mu^{M}_{B_2O_3}}{dx} \tag{A.26}$$

and for the perovskite phase (P):

$$j^{P}_{A^{3+}} = t^{P}_{A^{3+}}\frac{i_{cat}}{3F} - \frac{1}{(3F)^2}t^{P}_{A^{3+}}\sigma^{P}_{B^{3+}}\frac{d\mu^{P}_{A_2O_3}}{dx} \tag{A.27}$$

$$j^{P}_{B^{3+}} = t^{P}_{B^{3+}}\frac{i_{cat}}{3F} - \frac{1}{(3F)^2}t^{P}_{A^{3+}}\sigma^{P}_{B^{3+}}\frac{d\mu^{P}_{B_2O_3}}{dx} \tag{A.28}$$

and for the garnet phase (G):

$$j^{G}_{A^{3+}} = t^{G}_{A^{3+}}\frac{i_{cat}}{3F} - \frac{4}{5}\frac{1}{(3F)^2}t^{G}_{A^{3+}}\sigma^{G}_{B^{3+}}\frac{d\mu^{G}_{A_2O_3}}{dx} \tag{A.29}$$

$$j^{G}_{B^{3+}} = t^{G}_{B^{3+}}\frac{i_{cat}}{3F} - \frac{4}{3}\frac{1}{(3F)^2}t^{G}_{A^{3+}}\sigma^{G}_{B^{3+}}\frac{d\mu^{G}_{B_2O_3}}{dx} \tag{A.30}$$

The total ionic current density i_{cat} represents the effect of external electric field as a second driving force.

A.5. Chemical potential gradients of A_2O_3 and B_2O_3 in the product layers

The chemical potentials of components A_2O_3 and B_2O_3 at the boundaries of the product layers can be derived from the chemical equilibria in Eq. (1) to (3). For details, see the treatment of the only thermally-driven reaction [17]. The chemical potential gradients of components A_2O_3 and B_2O_3 in the product layers are calculated using the difference in the component chemical potentials at the adjacent phase boundaries and the product layer thicknesses Δx_M, Δx_P and Δx_G. For the monoclinic phase (M), one obtains:[3]

$$\frac{d\mu^{M}_{A_2O_3}}{dx} \approx \frac{\Delta\mu^{M}_{A_2O_3}}{\Delta x_M} = -\frac{\Delta_R G^{\circ}_M}{\Delta x_M} \tag{A.34}$$

$$\frac{d\mu^{M}_{B_2O_3}}{dx} \approx \frac{\Delta\mu^{M}_{B_2O_3}}{\Delta x_M} = 2\frac{\Delta_R G^{\circ}_M}{\Delta x_M} \tag{A.35}$$

for the perovskite phase (P):

$$\frac{d\mu^{P}_{A_2O_3}}{dx} \approx \frac{\Delta\mu^{P}_{A_2O_3}}{\Delta x_P} = -7\frac{\Delta_R G^{\circ}_P}{\Delta x_P} \tag{A.36}$$

$$\frac{d\mu^{P}_{B_2O_3}}{dx} \approx \frac{\Delta\mu^{P}_{B_2O_3}}{\Delta x_P} = 7\frac{\Delta_R G^{\circ}_P}{\Delta x_P} \tag{A.37}$$

and for the garnet phase (G):

$$\frac{d\mu^{G}_{A_2O_3}}{dx} \approx \frac{\Delta\mu^{G}_{A_2O_3}}{\Delta x_G} = -\frac{5}{3}\frac{\Delta_R G^{\circ}_G}{\Delta x_G} \tag{A.38}$$

$$\frac{d\mu^{G}_{B_2O_3}}{dx} \approx \frac{\Delta\mu^{G}_{B_2O_3}}{\Delta x_G} = \frac{\Delta_R G^{\circ}_G}{\Delta x_G} \tag{A.39}$$

Hereby, $\Delta_R G^{\circ}_i$ denote the free standard enthalpies according to the reactions in Eq. (1) to (3) (i = M, P, G).

[3] The free standard reaction enthalpies $\Delta_R G^{\circ}_M$, $\Delta_R G^{\circ}_P$ and $\Delta_R G^{\circ}_G$ for the partial reaction in Eq. (1), (2) and (3) can be calculated from the standard potentials of the neat product phases and starting materials:

$$\Delta_R G^{\circ}_M = \mu^{\circ}_{A_4B_2O_9} - (\mu^{\circ}_{A_2O_3} + 2\mu^{\circ}_{ABO_3}) \tag{A.31}$$

$$\Delta_R G^{\circ}_P = \mu^{\circ}_{ABO_3} - \frac{1}{7}(\mu^{\circ}_{A_4B_2O_9} + \mu^{\circ}_{A_3B_5O_{12}}) \tag{A.32}$$

$$\Delta_R G^{\circ}_G = \mu^{\circ}_{A_3B_5O_{12}} - (3\mu^{\circ}_{ABO_3} + \mu^{\circ}_{B_2O_3}) \tag{A.33}$$

A.6. Simultaneous growth of all product layers in an (external) electric field

The results stated in the preceding paragraphs regarding component gradients and cation fluxes can be combined to obtain expressions for the growth rate of each product layer. The rate equation for the growth of the monoclinic phase (M) in Eq. (A.40) is acquired by using Eq. (A.16) and the cation fluxes in Eq. (A.25) to (A.28):

$$\begin{aligned}\frac{1}{V_m^M}\frac{d(\Delta x_M)}{dt} &= -\frac{i_{cat}}{3F}\left(\frac{3}{2}t^M_{A^{3+}} - t^P_{A^{3+}} - \frac{1}{2}\right) + \frac{1}{(3F)^2}\left(\frac{9}{4}t^M_{A^{3+}}\sigma^M_{B^{3+}}\frac{d\mu^M_{A_2O_3}}{dx} - t^P_{A^{3+}}\sigma^P_{B^{3+}}\frac{d\mu^P_{A_2O_3}}{dx}\right)\\ &= \frac{i_{cat}}{3F}\left(\frac{3}{2}t^M_{B^{3+}} - t^P_{B^{3+}}\right) - \frac{1}{(3F)^2}\left(\frac{9}{8}t^M_{A^{3+}}\sigma^M_{B^{3+}}\frac{d\mu^M_{B_2O_3}}{dx} - t^P_{A^{3+}}\sigma^P_{B^{3+}}\frac{d\mu^P_{B_2O_3}}{dx}\right)\end{aligned} \tag{A.40}$$

In the case of the perovskite phase (P), Eq. (A.17) is combined with the cation fluxes in Eq. (A.25) to (A.30):

$$\begin{aligned}\frac{1}{V_m^P}\frac{d(\Delta x_P)}{dt} &= \frac{i_{cat}}{3F}\left(3t^M_{A^{3+}} - 7t^P_{A^{3+}} + 4t^G_{A^{3+}}\right) - \frac{1}{(3F)^2}\left(\frac{9}{2}t^M_{A^{3+}}\sigma^M_{B^{3+}}\frac{d\mu^M_{A_2O_3}}{dx} - 7t^P_{A^{3+}}\sigma^P_{B^{3+}}\frac{d\mu^P_{A_2O_3}}{dx} + \frac{16}{5}t^G_{A^{3+}}\sigma^G_{B^{3+}}\frac{d\mu^G_{A_2O_3}}{dx}\right)\\ &= -\frac{i_{cat}}{3F}\left(3t^M_{B^{3+}} - 7t^P_{B^{3+}} + 4t^G_{B^{3+}}\right) + \frac{1}{(3F)^2}\left(\frac{9}{4}t^M_{A^{3+}}\sigma^M_{B^{3+}}\frac{d\mu^M_{B_2O_3}}{dx} - 7t^P_{A^{3+}}\sigma^P_{B^{3+}}\frac{d\mu^P_{B_2O_3}}{dx} + \frac{16}{3}t^G_{A^{3+}}\sigma^G_{B^{3+}}\frac{d\mu^G_{B_2O_3}}{dx}\right)\end{aligned} \tag{A.41}$$

The growth rate of the garnet phase (G) in Eq. (A.42) is gained from Eq. (A.18) and the cation fluxes in Eq. (A.27) to (A.30):

$$\begin{aligned}\frac{1}{V_m^G}\frac{d(\Delta x_G)}{dt} &= \frac{i_{cat}}{3F}\left(t^P_{A^{3+}} - \frac{4}{3}t^G_{A^{3+}}\right) - \frac{1}{(3F)^2}\left(t^P_{A^{3+}}\sigma^P_{B^{3+}}\frac{d\mu^P_{A_2O_3}}{dx} - \frac{16}{15}t^G_{A^{3+}}\sigma^G_{B^{3+}}\frac{d\mu^G_{A_2O_3}}{dx}\right)\\ &= -\frac{i_{cat}}{3F}\left(t^P_{B^{3+}} - \frac{4}{3}t^G_{B^{3+}} + \frac{1}{3}\right) + \frac{1}{(3F)^2}\left(t^P_{A^{3+}}\sigma^P_{B^{3+}}\frac{d\mu^P_{B_2O_3}}{dx} - \frac{16}{9}t^G_{A^{3+}}\sigma^G_{B^{3+}}\frac{d\mu^G_{B_2O_3}}{dx}\right)\end{aligned} \tag{A.42}$$

If there is no growth of the adjacent phases and no (external) electric field, the chemical potential gradients of A_2O_3 and B_2O_3 in the adjacent phases and the total ionic current density i_{cat} in Eq. (A.40), (A.41) and (A.42) can be set to zero. Taking Eq. (A.34) to (A.39) into account, the complex expressions for the growth rate of a product layers are reduced to simple parabolic rate equations $d(\Delta x_i)/dt = k_i/\Delta x_i$ (i = M, P, G). The parabolic rate constants k_i for the independent (and uncoupled) growth can be identified as follows:[4]

$$k_M = -\frac{9}{4}V^M_m\frac{1}{(3F)^2}t^M_{A^{3+}}\sigma^M_{B^{3+}}\Delta_R G^\circ_M \tag{A.43}$$

$$k_P = -49V^P_m\frac{1}{(3F)^2}t^P_{A^{3+}}\sigma^P_{B^{3+}}\Delta_R G^\circ_P \tag{A.44}$$

$$k_G = -\frac{16}{9}V^G_m\frac{1}{(3F)^2}t^G_{A^{3+}}\sigma^G_{B^{3+}}\Delta_R G^\circ_G \tag{A.45}$$

and are also called rate constants of a “second kind” or “true” parabolic rate constants. If the driving force due to the chemical potenial gradients is small compared to the (external) electric field all chemical potential gradients of A_2O_3 and B_2O_3 in Eq. (A.40), (A.41) and (A.42) can be set to zero. The complex expression for the growth rate of a product layer is reduced to a simple linear rate equation $d(\Delta x_i)/dt = k^i_{elF}$ (i = M, P, G). New rate constants k^i_{elF} can be identified, describing the influence of the additional driving force:

$$k^M_{elF} = -\frac{i_{cat}}{3F}\left(\frac{3}{2}t^M_{A^{3+}} - t^P_{A^{3+}} - \frac{1}{2}\right)V^M_m = \frac{i_{cat}}{3F}\left(\frac{3}{2}t^M_{B^{3+}} - t^P_{B^{3+}}\right)V^M_m \tag{A.46}$$

$$k^P_{elF} = \frac{i_{cat}}{3F}\left(3t^M_{A^{3+}} - 7t^P_{A^{3+}} + 4t^G_{A^{3+}}\right)V^P_m = -\frac{i_{cat}}{3F}\left(3t^M_{B^{3+}} - 7t^P_{B^{3+}} + 4t^G_{B^{3+}}\right)V^P_m \tag{A.47}$$

$$k^G_{elF} = \frac{i_{cat}}{3F}\left(t^P_{A^{3+}} - \frac{4}{3}t^G_{A^{3+}}\right)V^G_m = -\frac{i_{cat}}{3F}\left(t^P_{B^{3+}} - \frac{4}{3}t^G_{B^{3+}} + \frac{1}{3}\right)V^G_m \tag{A.48}$$

Thus, Eq. (A.40) to (A.42), describing the simultaneous growth of the product layers under the influence of an (external) electric field can be rewritten in a simplified and condensed form when considering the parabolic rate constants in Eq. (A.43) to (A.45) and the new rate constants in Eq. (A.46) to (A.48), describing the effect of the superposed total ionic current:

$$\frac{1}{V^M_m}\frac{d(\Delta x_M)}{dt} = \frac{k^M_{elF}}{V^M_m} + \frac{k_M}{V^M_m}\frac{1}{\Delta x_M} - \frac{1}{7}\frac{k_P}{V^P_m}\frac{1}{\Delta x_P} \tag{A.49}$$

[4] In fact, the parabolic rate constants are averaged values, as the partial conductivities of the A^{3+} and B^{3+} cations may be composition/stoichiometry dependent.

$$\frac{1}{V_m^P}\frac{d(\Delta x_P)}{dt} = \frac{k_{elF}^P}{V_m^P} - 2\frac{k_M}{V_m^M}\frac{1}{\Delta x_M} + \frac{k_P}{V_m^P}\frac{1}{\Delta x_P} - 3\frac{k_G}{V_m^G}\frac{1}{\Delta x_G} \tag{A.50}$$

$$\frac{1}{V_m^G}\frac{d(\Delta x_G)}{dt} = \frac{k_{elF}^G}{V_m^G} - \frac{1}{7}\frac{k_P}{V_m^P}\frac{1}{\Delta x_P} + \frac{k_G}{V_m^G}\frac{1}{\Delta x_G} \tag{A.51}$$

This is a system of non-linear ODEs with constant coefficients. It cannot by solved analytically.

Appendix B. Supplementary data

Supplementary data to this article can be found online at https://doi.org/10.1016/j.ssi.2022.115978.

References

[1] H. Schmalzried, Chemical Kinetics of Solids, VCH-Verlagsgesellschaft, Weinheim, 1995.
[2] H. Schmalzried, Solid State Reactions, Verlag Chemie, Weinheim, 1981.
[3] M. Cologna, J.S. Francis, R. Raj, Field assisted and flash sintering of alumina and its relationship to conductivity and MGO-doping, J. Eur. Ceram. Soc. 31 (2011) 2827–2837, https://doi.org/10.1016/j.jeurceramsoc.2011.07.004.
[4] S.K. Jha, R. Raj, The effect of electric field on sintering and electrical conductivity of titania, J. Am. Ceram. Soc. 97 (2) (2014) 527–534, https://doi.org/10.1111/jace.12682.
[5] O. Guillon, J. Gonzalez-Julian, B. Dargatz, T. Kessel, G. Schierning, J. Räthel, M. Herrmann, Field-assisted sintering technology/spark plasma sintering: Mechanisms, materials, and technology developments, Adv, Eng. Mater. 16 (7) (2014) 830–849, https://doi.org/10.1002/adem.201300409.
[6] I.W.M. Brown, K.J.D. Mackenzie, Effect of electric fields on solid-state reactions between oxides - part 4 interdiffusion in polycrystalline calcium oxide and silicon dioxide pellets, J. Mater. Sci. 17 (12) (1982) 3663–3671.
[7] A.Y. Neiman, A.O. Krylov, V.A. Kuznetsov, Effect of an electric field on the solid-phase reactions between oxides, Russ. J. Phys. Chem. 59 (9) (1985) 1406–1407.
[8] M.T. Johnson, H. Schmalzried, C.B. Carter, The effect of an applied electric field on a heterogeneous solid-state reaction, Solid State Ionics 101 (2) (1997) 1327–1333.
[9] M.T. Johnson, S.R. Gilliss, C.B. Carter, Electric-field effects on reactions between oxides, Mater. Res. Soc. Symp. Proc. 481 (1998) 303–308.
[10] H. Schmalzried, S. Smolin, Ber. bunsenges, Phys. Chem 102 (1998) 1740.
[11] M.T. Johnson, C.B. Carter, H. Schmalzried, Behavior of mgfe$_{2}$o$_{4}$ films on MGO in an electric field, J. Am. Ceram. Soc. 83 (7) (2000) 1768–1772.
[12] E. Konisheva, E. Gorbunova, A. Neiman, Solid State, Ionics 141–142 (2001) 141–145.
[13] H. Schmalzried, On electric field induced processes in ionic compounds, Han'guk Seramik Hakhoechi 38 (6) (2001) 499–505.
[14] C. Korte, N. Ravishankar, C. Carter, H. Schmalzried, Kinetics of spinel formation in an external applied field, Solid State Ionics 148 (2002) 111.
[15] C. Korte, N.D. Zakharov, D. Hesse, Electric field driven solid state reactions - microscopic investigations of moving phase boundaries in the system MgO/$MgIn_2O_4$/In_2O_3, Phys. Chem. Chem. Phys. 5 (2003) 5530–5535.
[16] C. Korte, B. Franz, D. Hesse, Electric field driven solid state reactions - reaction kinetics and the influence of grain boundaries on the interface morphology in the system MgO/$MgIn_2O_4$/In_2O_3, Phys. Chem. Chem. Phys. 7 (2005) 413–420.
[17] C. Korte, B. Franz, Reaction kinetics in the system Y_2O_3/Al_2O_3 - A solid state reaction forming multiple product phases investigated by using thin film techniques, Solid State Ionics 368 (2021) 115699, https://doi.org/10.1016/j.ssi.2021.115699.
[18] N. Toropov, Phase Diagram for Ceramists Vol. 2, American Ceramic Society, Westerbille (OH), 1964, p. 96 (phase diagram of Y_2O_3-Al_2O_3) fig. 2344.
[19] A.S. Gandhi, C.G. Levi, Phase selection in precursor-derived yttrium aluminum garnet and related Al_2O_3-Y_2O_3 compositions, J. Mater. Res. 20 (4) (2005) 1017–1025, https://doi.org/10.1557/JMR.2005.0133.
[20] S. Lakiza, O. Fabrichnaya, C. Wang, M. Zinkevich, F. Aldinger, Phase diagram of the ZrO_2/Gd_2O_3/Al_2O_3 system, J. Eur. Ceram. Soc. 26 (2006) 233–246, https://doi.org/10.1016/j.jeurceramsoc.2004.11.011.
[21] U. Kolitsch, H. Seifert, F. Aldinger, Phase relationships in the system Gd_2O_3-Al_2O_3-SiO_2, J. Alloys Comp. 257 (1-2) (1997) 104–114, https://doi.org/10.1016/S0925-8388(96)03121-0.
[22] C. Wagner, The evaluation of data obtained with diffusion couples of binary single-phase and multiphase systems, Acta Metall. Mater. 17 (2) (1969) 99–107, https://doi.org/10.1016/0001-6160(69)90131-X.
[23] S.J. Schneider, R.S. Roth, J.L. Waring, Solid state reactions involving oxides of trivalent cations, J. Res. Natl. Bur. Stand. A: Phys. Chem. 65A (4) (1961) 345–374, https://doi.org/10.6028/jres.065A.037.
[24] J.R. Heffelfinger, C.B. Carter, Evolution of yttrium aluminum garnet films by solid-state reaction, MRS Proc. 317 (1993) 553–558, https://doi.org/10.1557/proc-317-553.
[25] T. Norby, P. Kofstad, Electrical conductivity of Y_2O_3 as a function of oxygen partial pressure in wet and dry atmospheres, J. Am. Cerum. Soc. 69 (11) (1986) 784–789.
[26] A.I. Kovrova, V.P. Gorelov, A.V. Kuz'min, B.A.-T. Melekh, The electric conductivity of poly- and singlecrystaline y_2o_3 in oxidative atmosphere, Russ. J. Electrochem. 54 (9) (2018) 733–740.
[27] O.T. Özkan, A.J. Moulson, The electrical conductivity of single-crystal and polycrystalline aluminium oxide, J. Phys. D: Appl. Phys. 3 (1970) 983–987.
[28] R. Brook, J. Yee, F. Kröger, Electrochemical cells and electrical conduction of pure and doped Al_2O_3, J. Am. Ceram Soc. 54 (9) (1971) 444–451.
[29] J. Yee, F.A. Kröger, Measurment of elecrtromotive force on Al_2O_3 - pitfalls and results, J. Am. Ceram. Soc. 56 (4) (1973) 189–191.
[30] F.G. Will, H.G. Delorenzi, K. Janora, Electrical conductivity and ionic transference measurements on single crystal alumina, Proc. Symp. Space Nucl. Power Syst. 1 (1990) 255–260.
[31] J. Pan, J. Öijerholm, A.B. Belonoshko, A. Rosengren, C. Leygraf, Self-diffusion activation energies in α-Al_2O_3 below 1000 ° - measurements and molecular dynamics calculation, Philos. Mag. Lett. 84 (12) (2004) 781–789, https://doi.org/10.1080/09500830500071051.
[32] J. Öijerholm, J. Pan, B. Jönsson, Influence of grain-size on ionic conductivity of pure and dense α-Al_2O_3 in the temperature range 400–1000 °, Mater. Sci. Forum 461-464 (2004) 865–874, https://doi.org/10.4028/www.scientific.net/MSF.461-464.865.
[33] L. Bates, J.E. Gamier, Electrical conductivity of $MgAl_2O_4$ and $Y_3Al_5O_{12}$, J. Am. Ceram. Soc. 64 (10) (1981) C138–C141, https://doi.org/10.1111/j.1151-2916.1981.tb10237.x.
[34] C. Schneider, W. Rasband, K. Eliceiri, NIH image to image j: 25 years of image analysis, Nat. Methods 9 (2012) 671–675, https://doi.org/10.1038/nmeth.2089.
[35] H. Schmalzried, T. Pfeiffer, The build-up of internal pressures during compoundformation, Z. Phys. Chem. N.F 148 (1986) 21–32.